

Implementations of the Universal Birkhoff Theory for Fast Trajectory Optimization

R. J. Proulx* and I. M. Ross†

Naval Postgraduate School, Monterey, CA 93943

This is part II of a two-part paper. Part I presented a universal Birkhoff theory for fast and accurate trajectory optimization. The theory rested on two main hypotheses. In this paper, it is shown that if the computational grid is selected from any one of the Legendre and Chebyshev family of node points, be it Lobatto, Radau or Gauss, then, the resulting collection of trajectory optimization methods satisfy the hypotheses required for the universal Birkhoff theory to hold. All of these grid points can be generated at an $\mathcal{O}(1)$ computational speed. Furthermore, all Birkhoff-generated solutions can be tested for optimality by a joint application of Pontryagin's- and Covector-Mapping Principles, where the latter was developed in Part I. More importantly, the optimality checks can be performed without resorting to an indirect method or even explicitly producing the full differential-algebraic boundary value problem that results from an application of Pontryagin's Principle. Numerical problems are solved to illustrate all these ideas. The examples are chosen to particularly highlight three practically useful features of Birkhoff methods: (1) bang-bang optimal controls can be produced without suffering any Gibbs phenomenon, (2) discontinuous and even Dirac delta covector trajectories can be well approximated, and (3) extremal solutions over dense grids can be computed in a stable and efficient manner.

I. Introduction

In [1], a new theory was advanced for fast and accurate trajectory optimization. This theory was based on the universal Birkhoff interpolants developed in [2]. The universal Birkhoff theory of [1] rested on two hypotheses; namely, that there exists a grid such that:

1. the a - and b -versions of the Birkhoff interpolant are equivalent; and,
2. the Birkhoff quadrature formula is accurate to within any given small $\epsilon > 0$.

In this paper, we first provide a proof of existence of such a grid; in fact, we show the existence of multiple grids that satisfy the two hypotheses. In addition, we provide implementation details for these particular choices of grid points and thereafter demonstrate the efficacy of the resulting Birkhoff methods by solving a set of illustrative problems.

As detailed in [1] and [2], the Birkhoff interpolants and the ensuing theory are different from the prior Birkhoff methods proposed in the literature [3–5]; in particular, it was shown in [1] that the universal interpolants designed in [2] also satisfy the covector mapping principle (CMP) [6–10], caveated by the two hypotheses noted earlier. That is, if a trajectory optimization method based on the new Birkhoff interpolants proposed in [2] is constructed, then, dualization and discretization can be commuted [6, 7, 10]. To explain, in simpler terms, why commutative operations in trajectory optimization are crucial [6] to generate the correct solution, consider the following simple univariate function,

$$g^N(x) := \frac{Nx + x^2}{N^2}, \quad x \in \mathbb{R}, \quad N \in \mathbb{N} \quad (1)$$

Suppose we minimize $g^N(x)$ with respect to x (holding N constant). It is straightforward to show that this yields,

$$\min_x g^N(x) = -\frac{1}{4} \quad (2)$$

Obviously, taking the limit of the left hand side of (2) as $N \rightarrow \infty$ generates,

$$\lim_{N \rightarrow \infty} \left(\min_x g^N(x) \right) = -\frac{1}{4} \quad (3)$$

*Research Professor, Control and Optimization Laboratories, Space Systems Academic Group

†Distinguished Professor and Program Director, Control and Optimization, Department of Mechanical and Aerospace Engineering

That is, minimizing $g^N(x)$ before taking the limit $N \rightarrow \infty$ produces the number, $-1/4$; however, if we reverse the operations, we get a different answer:

$$\lim_{N \rightarrow \infty} g^N(x) = 0 \quad (4a)$$

$$\min_x \left(\lim_{N \rightarrow \infty} g^N(x) \right) = 0 \quad (4b)$$

Obviously,

$$\lim_{N \rightarrow \infty} \min_x g^N(x) \neq \min_x \lim_{N \rightarrow \infty} g^N(x) \quad (5)$$

That is, lim and min are not commutative operations. Note that arg min and lim are also not commutative:

$$\arg \min_x \left(\lim_{N \rightarrow \infty} g^N(x) \right) \neq \lim_{N \rightarrow \infty} \left(\arg \min_x g^N(x) \right) \quad (6)$$

Trajectory optimization involves a number of commutative operations [6, 7, 10]; hence, it is crucial that any proposed trajectory optimization method satisfy the CMP. Production of covector mapping theorems for the original Birkhoff method used in [4, 5] parallels that of previous pseudospectral methods [11–14]; i.e., the development of intricate details that are specific to the different choices of grid points. In a quest for a more universal theory akin to the unified Lagrange pseudospectral (PS) method [15–17]; i.e., methods based on differentiation matrices [18–21], it was shown in [1] that the new Birkhoff interpolants proposed in [2] satisfy the CMP for any choice of grid points so long as two hypotheses are satisfied. With this perspective in mind, the main contributions of this paper are as follows:

1. A proof of existence of viable Birkhoff methods. This involves proving that a family of Legendre and Chebyshev grids (Lobatto, Radau and Gauss) satisfy the two hypotheses proposed in [1], and hence the CMP;
2. Implementation details of Birkhoff methods for the family of Legendre and Chebyshev grid points;
3. Results from select numerical problems to illustrate three features of the universal Birkhoff methods that are important in practical applications:
 - (a) Production of bang-bang-type solutions without suffering any Gibbs phenomenon despite the computational technique being based on Legendre/Chebyshev polynomials;
 - (b) Solution to state-constrained optimal control problems that require the existence and computation of discontinuous costates and Dirac-delta-type path covector trajectories; and
 - (c) Generation of solutions over very dense grids without suffering round-off errors or extensive preconditioning.

The preceding point 3c is particularly relevant when compared with PS methods based on Lagrange interpolants [18–21]. As noted in [1] and amplified in [2, 3], the main initial motivation for a Birkhoff theory was a need to produce a more perfect preconditioner [22, 23] to differentiation matrices. The search for a perfect preconditioner led to an “accidental” new starting point for PS theory and trajectory optimization itself [1]. Together with [1], this paper provides a more complete picture of this emerging new theory.

II. Legendre and Chebyshev Realizations of the Universal Birkhoff Theory

A practical realization of the universal Birkhoff theory for trajectory optimization narrows the selection of π^N to one that satisfies the two hypotheses of [1]. In this section, we show that the Gegenbauer family of Legendre and Chebyshev grids satisfy these hypotheses, thus paving the way for a practical computational framework. Note furthermore that the theory of [1] is based on an arbitrary grid and makes no assumptions of polynomial basis functions. In other words, no claim is made here that the Legendre and Chebyshev nodes are the only grid points that meet the criteria for the Birkhoff theory to hold.

For the purposes of brevity, we rely heavily on the recent developments from [2], together with some well-established results in spectral methods that use the theory of orthogonal polynomials [18, 19, 21, 24]. Furthermore, because this paper is a continuation of [1], we use previous symbols and notation without redefining them here.

In choosing Gegenbauer nodes, we hereafter constrain the computational time interval $[\tau^a, \tau^b]$ to the $[-1, 1]$ domain (i.e., $\tau^a = -1 = -\tau^b$). As a result, a domain transformation is needed to apply the ensuing method for a generic time interval $[t^a, t^b]$. This detail is discussed in Section III.

A. Definition and $\mathcal{O}(1)$ -Computation of Legendre and Chebyshev Grids

We begin by first noting that the Chebyshev grid points can be computed at an $\mathcal{O}(1)$ computational speed using the formula, $\tau_j = -\cos(\xi_j \pi)$, where ξ_j , $j = 0, \dots, N$ is determined based on the following selections [18–21]:

$$\text{Chebyshev-Gauss-Lobatto (CGL):} \quad \xi_j = \frac{j}{N} \quad (7a)$$

$$\text{Chebyshev-Gauss-Radau (CGR):} \quad \xi_j = \frac{2j}{2N+1} \quad (7b)$$

$$\text{Chebyshev-Gauss (CG):} \quad \xi_j = \frac{2j+1}{2N+2} \quad (7c)$$

The set of Legendre grid points are determined by the $(N+1)$ -zeroes of a function $z(\tau)$, where, $z(\tau)$ and the elements of the Legendre set are selected according to the following pairings [18–21]:

$$\text{Legendre-Gauss-Lobatto (LGL):} \quad z(\tau) = (1 - \tau^2) \dot{P}_N(\tau) \quad (8a)$$

$$\text{Legendre-Gauss-Radau (LGR):} \quad z(\tau) = P_N(\tau) + P_{N+1}(\tau) \quad (8b)$$

$$\text{Legendre-Gauss (LG):} \quad z(\tau) = P_{N+1}(\tau) \quad (8c)$$

where, P_N is a Legendre polynomial of order N . A quick examination of (8) appears to suggest that the computation of Legendre grids are significantly slower than $\mathcal{O}(1)$. In fact, this was true up until the pioneering work of Bogaert [25]. Bogaert's algorithm [25] computes all Legendre grids at an $\mathcal{O}(1)$ computational speed. With his advancement, all grid points denoted in (7) and (8) can be computed at an $\mathcal{O}(1)$ speed.

B. A Proof of Hypotheses 1 and 2 of [1] for a Select Family of Gegenbauer Grids

Gegenbauer polynomials (also known as ultraspherical polynomials [23]) are a subset of Jacobi polynomials that are orthogonal with respect to the weight function $(1 - \tau^2)^{\alpha-1/2}$. Setting $\alpha = 0$ yields Chebyshev polynomials (of the first kind) while $\alpha = 1/2$ generates Legendre polynomials.

To prove hypotheses 1 and 2, we need the two theorems presented below. As noted earlier, we direct the reader to multiple sources for more complete proofs of Theorems 1 and 2.

Theorem 1 ([2])

1. Let π^N be any one of the family of Chebyshev grid points given by (7). Then the Birkhoff quadrature weights are identical to the Clenshaw-Curtis (CC) weights for CGL nodes and Fejér's weights for CGR- and CG-grid points.
2. Let π^N be any one of the family of Legendre grid points given by (8). Then the Birkhoff quadrature weights are identical to the LGL, LGR and LG quadrature weights for the respective grid selections.

Remark 1 The importance of Theorem 1 is that no new formulas are needed for the computation of the Birkhoff quadrature weights provided the universal interpolants proposed in [2] are used. In sharp contrast, this result does not hold for the original Birkhoff interpolants proposed by Wang et al [3]. For instance, for an LGL grid, one needs to use the “Gauss-Lobatto-Legendre-Birkhoff” quadrature weights developed in [26].

Theorem 2 Let $y(\cdot) \in C[-1, 1]$. Define,

$$Q^N(y(\cdot)) := \sum_{i=0}^N y(\tau_i) w_i^{L/C} - \int_{-1}^1 y(\tau) d\tau \quad (9)$$

where $w_j^{L/C}$, $j = 0, \dots, N$ are the family of Legendre/Chebyshev quadrature weights defined in Theorem 1. Then, given any $\epsilon > 0$, there exists an $N_\epsilon \in \mathbb{N}$ such that for all $N \geq N_\epsilon$, $|Q^N(y(\cdot))| \leq \epsilon$

Proof. This theorem is well-known for the family of Legendre quadrature weights (Lobatto, Radau and Gauss). See, for example [18, 19, 21]. In the case of quadratures over a Chebyshev grid (Lobatto, Radau and Gauss), it was long thought that the results were not as accurate as those generated by Legendre node points [24, 27]. In fact, there is widespread belief that even among the Legendre family of quadrature weights, Gauss is the best. According to Trefethen [27], computations performed as far back as the 1960s showed that the Clenshaw-Curtis method yielded

results nearly as accurate as Gauss quadratures for the same number of node points. More recent research [27, 28] has placed these practical observations on a firm theoretical foundation where the purported differences in quadrature errors between Legendre and Chebyshev grids (be in Lobatto, Radau or Gauss) are either nonexistent or vanishingly small. Detailed proofs of these results can be found in [20, 24, 27, 28]. Note also that the statement of the current theorem is much weaker than a requirement that the Legendre/Chebyshev grid points have the same quadrature error, rather, the only requirement is that the errors be vanishingly small as N increases. \square

Proposition 1 (Proof of Hypothesis 1 of [1]) *Let π^N be any one of the family of Legendre/Chebyshev grids from Theorem 1. Then, Hypothesis 1 of [1] holds; i.e., the a - and b -forms of the Birkhoff interpolants given in [1] (and [2]) are equivalent.*

Proof. Let $[-1, 1] \ni \tau \mapsto y(\tau) \in \mathbb{R}$ be a given bounded differentiable function. Then, from their defining equations given in [1], it follows that,

$$I_a^N y(-1) = y(-1) \quad \text{and} \quad I_b^N y(1) = y(1) \quad (10)$$

Hence,

$$I_b^N y(\tau) - I_a^N y(\tau) = y(1) - y(-1) + \sum_{j=0}^N \dot{y}(\tau_j) (B_j^b(\tau) - B_j^a(\tau)) \quad (11)$$

From Proposition 3 of [2] (see also Lemma 2 in [1]), (11) can be written as,

$$I_b^N y(\tau) - I_a^N y(\tau) = y(1) - y(-1) - \sum_{j=0}^N \dot{y}(\tau_j) w_j^B \quad (12)$$

From Theorem 1, (12) can be written as,

$$I_b^N y(\tau) - I_a^N y(\tau) = y(1) - y(-1) - \sum_{j=0}^N \dot{y}(\tau_j) w_j^{L/C} \quad (13)$$

From Theorem 2, (13) can be written as,

$$I_b^N y(\tau) - I_a^N y(\tau) = y(1) - y(-1) - \int_{-1}^1 \dot{y}(\tau) d\tau + \epsilon^N \quad (14)$$

where ϵ^N is vanishingly small as $N \rightarrow \infty$. The result then follows by evaluating the integral in (14). \square

Proposition 2 (Proof of Hypothesis 2 of [1]) *Theorem 2 is a proof of Hypothesis 2 of [1] for the choices of π^N denoted in Theorem 1.*

C. Impact of Selecting Legendre/Chebyshev- Gauss, Gauss-Radau and Gauss-Lobatto Grids

The results of subsection B suggest that there is virtually no difference in selecting any one of the six families of grid points denoted in Theorem 1. Although this is true in principle, we note the following caveats that are specific to computational optimal control:

1. **Legendre/Chebyshev-Gauss grid:** A Gauss grid does not include the boundary points, -1 and 1 . Consequently, if the boundary conditions are imposed at the boundary points, the controls at the boundaries are unavailable. Hence, to perform a feasibility test (see Section III), some form of control extrapolation is needed.
2. **Legendre/Chebyshev-Gauss-Radau grid:** A Radau grid does not include one of the boundary points. Thus, either the initial- or final-value of the control is unavailable. Extrapolation is needed in both cases.
3. **Legendre/Chebyshev-Gauss-Lobatto grid:** A Lobatto grid includes both boundary points; hence, both the initial and final values of the controls are available without introducing any adhoc extrapolation rules.

Although the caveats noted above are relatively minor with regards to a Birkhoff implementation, note that these small differences are amplified to a detrimental effect with regards to Gauss or Radau selections when a Lagrange PS method is chosen for trajectory optimization [13, 17, 29]. This is the main reason why Gauss/Radau grids have not been selected for flight implementations [17, 30–32].

Remark 2 *Following [1–3], we classify PS methods based on the type of interpolants used; i.e., Lagrange or Birkhoff. Secondary classification follows the well-established convention [18–20] of basing it on the type of computational basis functions used; e.g., Legendre, Chebyshev etc. A tertiary level of classification is based on the type of grid used with the associated computational basis function; e.g., Lobatto, Radau, Gauss.*

III. Legendre/Chebyshev Implementations of Birkhoff Optimal Control Theory

A Legendre/Chebyshev implementation of the universal Birkhoff theory for optimal control [1] can now be performed by incorporating the results of Section II with those from [1] and [2]. Additional details of implementation follow from relevant optimal control programming techniques that are extensively described elsewhere [4,5,17,33–35]. Hence, we limit the scope of this section to just those details that are specific only to the new Birkhoff method.

A. A Generic Optimal Control Problem Formulation

A fairly generic optimal control problem may be described in the form of following compact format [7]:

$$(P) \begin{cases} \text{Minimize} & J[\mathbf{x}(\cdot), \mathbf{u}(\cdot), t^a, t^b, \mathbf{p}] = E(\mathbf{x}(t^a), \mathbf{x}(t^b), t^a, t^b, \mathbf{p}) \\ & + \int_{t^a}^{t^b} F(\mathbf{x}(t), \mathbf{u}(t), t, \mathbf{p}) dt \\ \text{Subject to} & \dot{\mathbf{x}}(t) = \mathbf{f}(\mathbf{x}(t), \mathbf{u}(t), t, \mathbf{p}) \\ & \mathbf{e}^L \leq \mathbf{e}(\mathbf{x}(t^a), \mathbf{x}(t^b), t^a, t^b, \mathbf{p}) \leq \mathbf{e}^U \\ & \mathbf{h}^L \leq \mathbf{h}(\mathbf{x}(t), \mathbf{u}(t), t, \mathbf{p}) \leq \mathbf{h}^U \end{cases} \quad (15)$$

where, the symbol $N_{(\cdot)} \in \mathbb{N}$ represents the number of variables or equations implied by its subscript. We assume $t^b > t^a$ and \mathbf{p} is a static optimization parameter that must be determined jointly with $\mathbf{x}(\cdot)$ and $\mathbf{u}(\cdot)$ in addition to the clock times, t^a and t^b . The cost functional J is given in the “Bolza” or standard form [7] where, E and F are the the endpoint- and running-cost functions respectively. The running cost, F , pairs with the dynamics data function, \mathbf{f} , via the adjoint covector (costate), $\boldsymbol{\lambda}$, to form the (Pontryagin) Hamiltonian function,

$$H(\boldsymbol{\lambda}, \mathbf{x}, \mathbf{u}, t, \mathbf{p}) := F(\mathbf{x}, \mathbf{u}, t, \mathbf{p}) + \boldsymbol{\lambda}^T \mathbf{f}(\mathbf{x}, \mathbf{u}, t, \mathbf{p}) \quad (16)$$

The function, E , pairs with the endpoint constraint function, \mathbf{e} , via the events covector, $\boldsymbol{\nu}$, to form the endpoint Lagrangian [7]:

$$\overline{E}(\boldsymbol{\nu}, \mathbf{x}^a, \mathbf{x}^b, t^a, t^b, \mathbf{p}) := E(\mathbf{x}^a, \mathbf{x}^b, t^a, t^b, \mathbf{p}) + \boldsymbol{\nu}^T \mathbf{e}(\mathbf{x}^a, \mathbf{x}^b, t^a, t^b, \mathbf{p}) \quad (17)$$

Likewise, the path constraint function, \mathbf{h} , pairs with H via the path covector, $\boldsymbol{\mu}$, to form the Lagrangian of the Hamiltonian; i.e., the Lagrangian associated with the Hamiltonian minimization condition (HMC) [7],

$$\overline{H}(\boldsymbol{\mu}, \boldsymbol{\lambda}, \mathbf{x}, \mathbf{u}, t, \mathbf{p}) := H(\boldsymbol{\lambda}, \mathbf{x}, \mathbf{u}, t, \mathbf{p}) + \boldsymbol{\mu}^T \mathbf{h}(\mathbf{x}, \mathbf{u}, t, \mathbf{p}) \quad (18)$$

The superscripts L and U in (15) denote their lower and upper bounds on the values of the functions \mathbf{e} and \mathbf{h} .

Additional cost functionals and constraints may be added to further generalize (15); however, it will be apparent later that such additions can be easily incorporated into the Birkhoff theory using the fundamentals covered in [1] and this section. For similar reasons, incorporating “phases” in generalizing (15) follows in quite a straightforward manner based on the results of [12,33,34,36,37]. As noted in [1] and elsewhere [4,5,13], such details, while important, are more distracting to the presentation of the core fundamentals.

B. Legendre/Chebyshev Details for Birkhoff Optimal Control Programming

To apply the theory from [1] for a selection of Legendre/Chebyshev grid points to solve Problem (P), two additional ingredients are necessary: (1) an invertible and differentiable domain transformational mapping (i.e., a diffeomorphism) from the $[-1, 1]$ to $[t^a, t^b]$, and (2) explicit computational formulas for producing $\mathbf{B}^\theta(\pi^N)$, $\theta \in \{a, b\}$ and $\mathbf{w}_B(\pi^N)$ for the choices of π^N denoted in Theorem 1.

1. Domain Transformation

Let, Γ be a differentiable, invertible function with arguments $(\tau, t^a, t^b; \mathbf{p}_t)$, such that [7, 17, 35],

$$t = \Gamma(\tau, t^a, t^b; \mathbf{p}_t) \quad (19)$$

where, $t^a = \Gamma(-1, t^a, t^b; \mathbf{p}_t)$, $t^b = \Gamma(1, t^a, t^b; \mathbf{p}_t)$ and $\mathbf{p}_t \in \mathbb{R}^{N_{p_t}}$ is a parameter that can be selected a priori or optimized. If \mathbf{p}_t is optimized, the subsequent grid is adaptive [17, 38]; if Γ is nonlinear, the grid can be designed to

support anti-aliasing [39, 40] and assist in the resolution of the system trajectory [7, 38, 40]. The simplest choice of Γ for a finite horizon problem is the affine function,

$$t = \Gamma(\tau, t^a, t^b; \mathbf{p}_t) \equiv \Gamma_{aff}(\tau, t^a, t^b) := \left(\frac{t^b - t^a}{2} \right) \tau + \left(\frac{t^b + t^a}{2} \right) \quad (20)$$

See [7, 41–43] on how to select Γ for infinite horizon problems. With a suitable choice of Γ , Problem (P) is easily transformed to the computational domain $[-1, 1]$ by substituting (19) in (15). The integral and the differential equations in (15) transform according to,

$$\int_{t^a}^{t^b} F(\mathbf{x}(t), \mathbf{u}(t), t, \mathbf{p}) dt = \int_{-1}^1 \gamma F(\mathbf{x}(\tau), \mathbf{u}(\tau), \Gamma, \mathbf{p}) d\tau \quad (21a)$$

$$\frac{d\mathbf{x}(\tau)}{d\tau} = \gamma \mathbf{f}(\mathbf{x}(\tau), \mathbf{u}(\tau), \Gamma, \mathbf{p}) \quad (21b)$$

where, $\gamma = \left(\frac{d\Gamma}{d\tau} \right)$. In (21) we have abused notation for expediency. The symbols $\mathbf{x}(\tau)$ and $\mathbf{u}(\tau)$ should be written more technically as $\mathbf{x}(\Gamma(\tau, t^a, t^b; \mathbf{p}_t))$ and $\mathbf{u}(\Gamma(\tau, t^a, t^b; \mathbf{p}_t))$ respectively. Likewise, the dependence of γ on t^a, t^b and possibly \mathbf{p}_t is suppressed for convenience.

2. Computation of $\mathbf{B}^\theta(\pi^N)$ and $\mathbf{w}_B(\pi^N)$

Efficient computational procedures for computing $\mathbf{B}^\theta(\pi^N)$, $\theta \in \{a, b\}$ over a generic grid, π^N , are provided in [2]. In particular, [2] provides explicit computational formulas for $\mathbf{B}^\theta(\pi^N)$ when π^N is chosen in accordance with the selection of grids denoted in Theorem 1.

To compute $\mathbf{w}_B(\pi^N)$, the following options are available:

1. If π^N is chosen to be an LGL or a CGL grid, then the last row of \mathbf{B}^a turns out to be exactly equal to \mathbf{w}_B [2]; hence, no new computations are necessary.
2. If π^N is chosen to be a non-Lobatto grid (i.e, Radau or Gauss), then additional computations must be performed to produce \mathbf{w}_B . The software, `chebfun` [44], implements fast and efficient formulas for computing these weights (cf. Theorem 1).

To verify and validate these computation, the following checks may be performed:

1. $B_j^a(\tau_k) - B_j^b(\tau_k) = w_j^B$, $j, k = 0, \dots, N$; see Proposition 3 in [2].
2. If π^N is selected to be an LGL or a CGL grid, then, $\mathbf{B}^a = -I^\diamond \mathbf{B}^b I^\diamond$, where, I^\diamond is the exchange matrix; see Proposition 5 in [2].

3. Matrix-Vector Mathematical Programming Problem Formulation

As noted elsewhere [5, 35, 45–48], discretizing Problem (P) (by any valid method) generates an information-rich mathematical programming problem that is better described as a Hamiltonian programming [35, 47, 48] problem rather than a generic nonlinear programming problem. To preserve this Hamiltonian structure, we follow [4, 35] and define three matrices according to:

$$\mathbf{X} := [\mathbf{x}_0, \mathbf{x}_1, \dots, \mathbf{x}_N] \in \mathbb{R}^{N_x \times (N+1)} \quad (22a)$$

$$\mathbf{V} := [\mathbf{v}_0, \mathbf{v}_1, \dots, \mathbf{v}_N] \in \mathbb{R}^{N_v \times (N+1)} \quad (22b)$$

$$\mathbf{U} := [\mathbf{u}_0, \mathbf{u}_1, \dots, \mathbf{u}_N] \in \mathbb{R}^{N_u \times (N+1)} \quad (22c)$$

where, $\mathbf{x}_k \in \mathbb{R}^{N_x}$, $\mathbf{v}_k \in \mathbb{R}^{N_v}$, $\mathbf{u}_k \in \mathbb{R}^{N_u}$, $k = 0, 1, \dots, N$. This format allows us to preserve the structural nature of (15); for instance, the path constraint function can be evaluated over the transformed grid, $\Gamma^N = \Gamma(\pi^N, t^a, t^b, \mathbf{p})$, by overloading \mathbf{h} according to [7, 35],

$$\mathbf{h}(\mathbf{x}(t), \mathbf{u}(t), t, \mathbf{p}) \mapsto \mathbf{h}(\mathbf{X}, \mathbf{U}, \Gamma^N, \mathbf{p}) \in \mathbb{R}^{N_h \times (N+1)} \quad (23)$$

Using similar constructs and the framework of [1], it is straightforward to show that the α -form of the universal Birkhoff discretization of Problem (P) can be framed as:

$$\begin{aligned}
& \mathbf{X} \in \mathbb{R}^{N_x \times (N+1)}, \quad \mathbf{U} \in \mathbb{R}^{N_u \times (N+1)}, \quad \mathbf{V} \in \mathbb{R}^{N_x \times (N+1)} \\
& t^a \in \mathbb{R}, \quad t^b \in \mathbb{R}, \quad \mathbf{x}^a \in \mathbb{R}^{N_x}, \quad \mathbf{x}^b \in \mathbb{R}^{N_x} \\
& \left\{ \begin{array}{ll} \text{Minimize} & J^N[\mathbf{X}, \mathbf{U}, \mathbf{V}, \mathbf{x}^a, \mathbf{x}^b, t^a, t^b] := E(\mathbf{x}^a, \mathbf{x}^b, t^a, t^b) \\ & + \gamma \mathbf{w}_B^T(\pi^N) F(\mathbf{X}, \mathbf{U}, \Gamma^N, \mathbf{p}) \\ \text{Subject to} & \mathbf{A}_a(\pi^N) \begin{bmatrix} \mathbf{X}^T \\ \mathbf{V}^T \end{bmatrix} - \mathbf{C}_a^N \begin{bmatrix} \mathbf{x}^a \\ \mathbf{x}^b \end{bmatrix} = \mathbf{0} \\ & \mathbf{V} = \gamma \mathbf{f}(\mathbf{X}, \mathbf{U}, \Gamma^N, \mathbf{p}) \\ & e^L \leq e(\mathbf{x}^a, \mathbf{x}^b, t^a, t^b, \mathbf{p}) \leq e^U \\ & \mathbf{h}^L \leq \mathbf{h}(\mathbf{X}, \mathbf{U}, \Gamma^N, \mathbf{p}) \leq \mathbf{h}^U \end{array} \right. \quad (24)
\end{aligned}$$

where, $\mathbf{A}_a(\pi^N)$ is an $((N+2) \times 2(N+1))$ -matrix that depends upon the choice of π^N ,

$$\mathbf{A}_a(\pi^N) := \begin{bmatrix} \mathbf{I}^N & -\mathbf{B}^a(\pi^N) \\ \mathbf{0}^T & \mathbf{w}_R^T(\pi^N) \end{bmatrix} \quad (25)$$

$\mathbf{0}$ is an $((N+1) \times 1)$ vector of zeros, and \mathbf{C}_a^N is an $((N+2) \times 2)$ -matrix given by,

$$\mathbf{C}_a^N := \begin{bmatrix} \mathbf{b} & \mathbf{0} \\ -1 & 1 \end{bmatrix} \quad (26)$$

The symbol $\mathbf{P}_a(\pi^N)$ used in (24) is the vectorized version of P_a^N defined in [1]. In (24) it is written more elaborately as $\mathbf{P}_a(\pi^N)$ to signify its dependence on the choice of π^N . See also [5] for additional details on efficient matrix methods for organizing variables.

Remark 3 Similar to the development of (24), other forms of $\mathbf{P}_\theta(\pi^N)$, $\theta \in \{b, a^*, b^*\}$ [1] can be generated. Because the process is quite similar, they are not detailed here for brevity but depicted in Fig. 1. It is apparent from Fig. 1 that a multiplicity of possibilities can be easily generated using the results of Section II and the theory developed in [1]. See also Remark 2 in the context of Fig. 1.

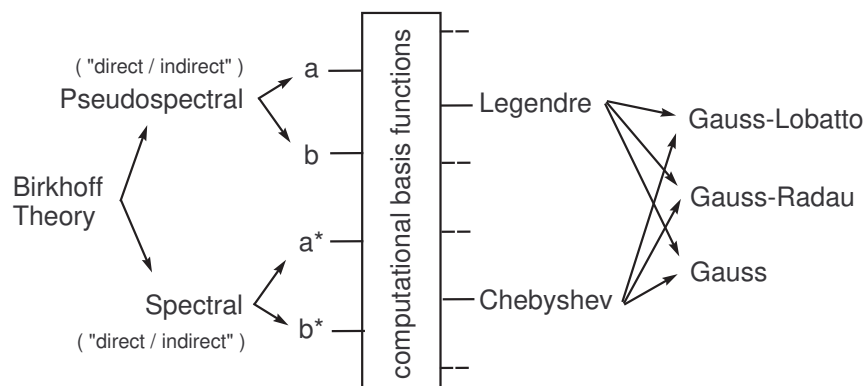


Figure 1. Schematic for the flow of the new Birkhoff theory for trajectory optimization: from its origin to various primal/dual implementations; figure adapted from [35].

Once a computable version of Problem ($\mathbf{P}_\theta(\pi^N)$), $\theta \in \{a, b, a^*, b^*\}$ is formulated, then the entire power of the universal Birkhoff theory [1] can be brought to bear on solving Problem (\mathbf{P}). A candidate solution obtained by such a process can then be subjected to a rigorous battery of Birkhoff-independent verification and validation tests. These tests are described in the next section and illustrated via sample problems and solutions in Section V.

IV. Birkhoff-Independent Verification and Validation Tests

Suppose one is presented with a candidate optimal control trajectory, $t \mapsto \mathbf{u}(t) \in \mathbb{R}^{N_u}$, that purports to solve Problem (P). Regardless of how $\mathbf{u}(\cdot)$ was obtained, it is obvious that an optimal trajectory must satisfy the necessary conditions for optimality (otherwise, these conditions would be unnecessary). A precursor to optimality is primal feasibility. This is simply because if the candidate control trajectory is not feasible, it is certainly not optimal.

A. Primal Feasibility Tests

In any grid-based computation, the control signal is given by the set of points,

$$\{(t_i, \mathbf{u}(t_i)) \in \mathbb{R} \times \mathbb{R}^{N_u}, i = 0, \dots, N\} \quad (27)$$

Frequently, but not always, this is associated with a state solution over the same grid:

$$\{(t_i, \mathbf{x}(t_i)) \in \mathbb{R} \times \mathbb{R}^{N_x}, i = 0, \dots, N\} \quad (28)$$

A claim of primal feasibility based solely on the pairs $(\mathbf{x}(t_i), \mathbf{u}(t_i), i = 0, \dots, N)$ satisfying all the constraints associated with Problem (P) (cf. (15), with \mathbf{p} temporarily ignored for convenience) is frequently false [7, 39, 40]. To clarify this statement, we use the following definition:

Definition 1 A state-control function pair, $t \mapsto (\mathbf{x}^\sharp(t), \mathbf{u}^\sharp(t)) \in \mathbb{R}^{N_x} \times \mathbb{R}^{N_u}$ and a parameter \mathbf{p}^\sharp are said to be primal feasible if they satisfy all the constraints associated with Problem (P).

Note that Definition 1 is not based on (27) and (28). To obtain a *certificate of feasibility* for (27), one must first generate a continuous-time control signal $t \mapsto \mathbf{u}^\sharp(t)$. This can be easily done by using the formula,

$$\mathbf{u}^\sharp(t) = \sum_{i=0}^N \mathbf{u}(t_i) \zeta_i(t) \quad (29)$$

where, $\zeta(t)$ is any valid interpolating function; i.e., one that satisfies the condition $\zeta_i(t_j) = \delta_{ij}$. In practice, it is highly desirable for $\zeta(t)$ to be agnostic to the method on how (27) was created so that there is an additional layer of independence in the tests to be performed. See, for example [49] for a detailed discussion on choosing $\zeta_i(t)$ for a practical problem pertaining to a trans-Earth Lunar mission. A state trajectory, $t \mapsto \mathbf{x}^\sharp(t)$, associated with (29) can now be obtained quite easily by solving the initial value problem (IVP),

$$\dot{\mathbf{x}}^\sharp = \mathbf{f}(\mathbf{x}^\sharp, \mathbf{u}^\sharp(t)) \equiv \mathbf{g}(\mathbf{x}^\sharp, t), \quad \mathbf{x}^\sharp(t^a) = \mathbf{x}^a \quad (30)$$

Thus, a procedure for a primal feasibility test is as follows:

1. Solve Problem $(P_\theta(\pi^N))$ to generate (27).
2. Select a $\zeta(t)$ (typically, piecewise linear) to construct (29).
3. Solve the IVP given by (30) to generate $t \mapsto \mathbf{x}^\sharp(t)$.
4. If $t \mapsto (\mathbf{x}^\sharp(t), \mathbf{u}^\sharp(t))$ is primal feasible (cf. Definition 1), then we declare the control solution given by (27) to be feasible.

Remark 4 For flight implementation, it is irrelevant how (27) was generated. In typical flight operations [17, 30–32, 50, 51], (29) is used with some $\zeta_i(t)$ (e.g. piecewise linear or zero-order-hold) to solve (30) (via, for example, a fourth-order Runge-Kutta integrator) to perform an independent verification of (primal) feasibility. Such tests are performed in all examples reported in Section V.

Remark 5 It is worth emphasizing at this point that a grid-based control solution (in the format of (27)) obtained by a Birkhoff method is not necessarily of polynomial origin even if the underlying computation of a Birkhoff matrix is based on orthogonal polynomials. In fact, as explained in Section III of [1], $\mathbf{u}(t_i)$ is frequently not of polynomial origin.

See [7] and [35] for additional details and the impact of using (29) and (30) with regards to practically achievable tolerances on constraint violations.

B. Optimality Tests via Pontryagin's Principle

A necessary condition is based on the principle that a candidate primal-feasible solution has been found. Suppose that the tests indicated in subsection A have been successfully completed. If this feasible solution is purportedly optimal, then it must necessarily satisfy a set of conditions for optimality. This set of necessary conditions is given by Pontryagin's principle [7]. The necessary conditions for Problem (P) are given by [7]:

$$\text{Hamiltonian Minimization Condition:} \quad \mathbf{u}(t) = \arg \min_{\mathbf{u}(t) \in \mathbb{U}(t, \mathbf{x}(t))} H(\boldsymbol{\lambda}(t), \mathbf{x}(t), \mathbf{u}(t), t, \mathbf{p}) \quad (31a)$$

$$\text{Adjoint equation:} \quad -\dot{\boldsymbol{\lambda}}(t) = \partial_{\mathbf{x}} \overline{H}(\boldsymbol{\mu}(t), \boldsymbol{\lambda}(t), \mathbf{x}(t), \mathbf{u}(t), t, \mathbf{p}) \quad (31b)$$

$$\text{Hamiltonian Value Conditions:} \quad \mathcal{H}[\text{at } t^\theta] = \pm \partial_{t^\theta} \overline{E}(\boldsymbol{\nu}, \mathbf{x}^a, \mathbf{x}^b, t^a, t^b, \mathbf{p}) \quad \theta \in \{a, b\} \quad (31c)$$

$$\begin{aligned} \text{Hamiltonian Evolution Equation:} \quad & \frac{dH(\boldsymbol{\lambda}(t), \mathbf{x}(t), t, \mathbf{p})}{dt} \\ &= \frac{\partial \overline{H}(\boldsymbol{\mu}(t), \boldsymbol{\lambda}(t), \mathbf{x}(t), \mathbf{u}(t), t, \mathbf{p})}{\partial t} \end{aligned} \quad (31d)$$

$$\text{Transversality Condition:} \quad \boldsymbol{\lambda}(t^\theta) = \mp \partial_{\mathbf{x}^\theta} \overline{E}(\boldsymbol{\nu}, \mathbf{x}^a, \mathbf{x}^b, t^a, t^b, \mathbf{p}) \quad \theta \in \{a, b\} \quad (31e)$$

$$\begin{aligned} \text{Optimal Parameter Condition:} \quad & \partial_{\mathbf{p}} \overline{E}(\boldsymbol{\nu}, \mathbf{x}^a, \mathbf{x}^b, t^a, t^b, \mathbf{p}) \\ &+ \int_{t^a}^{t^b} \partial_{\mathbf{p}} \overline{H}(\boldsymbol{\mu}(t), \boldsymbol{\lambda}(t), \mathbf{x}(t), \mathbf{u}(t), t, \mathbf{p}) dt = \mathbf{0} \end{aligned} \quad (31f)$$

where, $\boldsymbol{\nu}$ and $\boldsymbol{\mu}(t)$ satisfy the complementarity conditions denoted symbolically as [7],

$$\boldsymbol{\nu} \dagger \mathbf{e}(\mathbf{x}^a, \mathbf{x}^b, t^a, t^b, \mathbf{p}), \quad \boldsymbol{\mu}(t) \dagger \mathbf{h}(\mathbf{x}(t), \mathbf{u}(t), t, \mathbf{p}) \quad \forall t \in [t^a, t^b] \quad (32)$$

As explained in Section I, it is necessary for certain operators to be commutative because an absence of commutativity may generate the converged but wrong answer; see [6] for details. The required commutativity between dualization and discretization is indeed the CMP and is illustrated in Fig. 3 of [1]. Because the Legendre/Chebyshev grids denoted in Theorem 1 satisfy the two hypotheses required for the universal Birkhoff theory to hold, the covector mapping theorems of [1] hold for this selection of node points. Consequently, all the conditions stipulated in (31) and (32) must hold if a candidate control solution given by (27) is to be optimal. Such primal-feasibility- and optimality tests are illustrated in Section V.

V. Illustrative Problems and Solutions

As implied by the theoretical foundations presented in [1], a computational method based on the universal Birkhoff theory should have no major technical roadblocks in solving a wide variety of optimal control problems. The main caveat for the theory to hold is the two hypotheses put forth in [1]. Having shown in Section II that these hypotheses are indeed satisfied for the family of Legendre and Chebyshev grids denoted in Theorem 1, we now demonstrate various aspects of the numerical performance of a Birkhoff PS method via the implementations described in Section III. For the purpose of brevity, we limit the presentation of the numerical performance to CGL grids while noting that similar results were obtained for the LGL grid.

In the following subsections, we solve a selection of problems to demonstrate the following features that are important in solving application problems in aerospace and mechanical engineering:

1. Production of a discontinuous optimal control solution without the need for introducing PS knots [33, 34, 36] for mesh refinement;
2. Solution to a state-constrained problem that involves shifted Dirac-delta-type functions (of atomic measure) for its path covector trajectory; and,
3. Generation of a highly oscillatory trajectory, with $N > 1000$, without facing technical roadblocks involving high condition numbers, round-off errors or instability issues.

A. A Trajectory Optimization Problem With Control Jumps

The collection of moon-landing problems described in [7] are nonlinear trajectory optimization problems with control discontinuities. A particular one-degree-of-freedom version of this problem [52], with moon's gravity normalized to

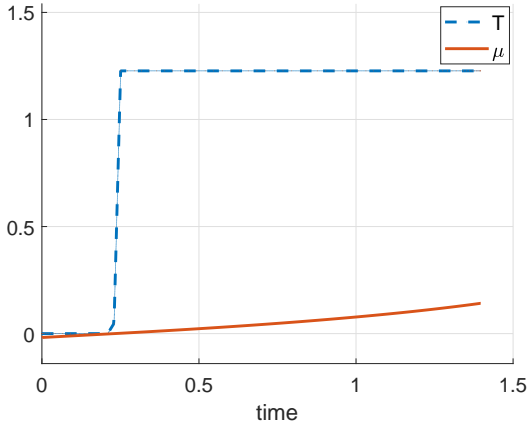
unity, is posed in [7] as:

$$\begin{aligned}
 \mathbf{x} &:= (h, v, m) \in \mathbb{R}^3, \quad \mathbf{u} := T \in \mathbb{R} \\
 (ML_1) \left\{ \begin{array}{ll} \text{Minimize} & J[\mathbf{x}(\cdot), \mathbf{u}(\cdot), t_f] := \int_{t^a}^{t_f} \frac{T(t)}{2.349} dt \\ \text{Subject to} & \begin{aligned} \dot{h}(t) &= v(t) \\ \dot{v}(t) &= -1 + \frac{T(t)}{m(t)} \\ \dot{m}(t) &= -\frac{T(t)}{2.349} \\ t_0 &= 0 \\ (h(t_0), v(t_0), m(t_0)) &= (1, -0.783, 1) \\ (h_f, v_f) &= (0, 0) \\ 0 \leq T &\leq 1.227 \end{aligned} \end{array} \right. \quad (33)
 \end{aligned}$$

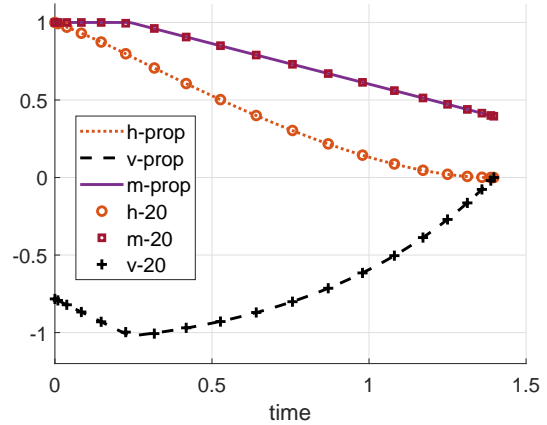
A set of near-universal checkable conditions for optimality is the KKT conditions associated with minimizing the Hamiltonian given by (31a). For Problem (ML_1) , the complementarity condition (see (32)) associated with minimizing the Hamiltonian is given by [7],

$$\mu(t) \begin{cases} \leq 0, & \text{if } T(t) = 0 \\ \geq 0, & \text{if } T(t) = 1.227 \end{cases} \quad (34)$$

where $\mu(t) \in \mathbb{R}$ is the instantaneous value of the path covector associated with the thrust -limiting path constraint, $0 \leq T(t) \leq 1.227$. It can be shown [7] that the optimal solution to this problem comprises only bang-bang controls. A linearly-interpolated 80-node Birkhoff solution for the thrust profile is shown in Fig. 2.a) along with a similar 80-node plot of the path covector trajectory, $t \mapsto \mu(t)$. From this plot, it is apparent that:



a) Birkhoff-theoretic bang-bang thrust control profile and its corresponding switching covector trajectory, $t \mapsto \mu(t)$.



b) Primal feasible solution obtained via solving (30) overlaid with a 20-node solution.

Figure 2. Candidate optimal solution to Problem (ML_1) .

1. The on-off nature of the optimal thrust solution is well-captured by a Birkhoff solution (without introducing traditional mesh refinement techniques [33, 34, 36];
2. There is no Gibbs phenomenon in the bang-bang nature of the thrust profile; and
3. The optimality condition given by (34) is satisfied.

Fig. 2.b) shows the state trajectories obtained by integrating (using `ode45` in MATLAB) the differential equations using the Birkhoff thrust profile (of Fig. 2.a)). These are denoted as (h, v, m) -prop in Fig. 2.b). These plots are in accordance with solving (30) for an “independent” verification of primal feasibility; see Remark 4. Also shown in Fig. 2.b) are the Birkhoff-generated state solutions for $N = 20$ denoted as (h, v, m) -20. It is apparent from this figure that the Birkhoff solution for as little as $N = 20$ has indeed converged, thus demonstrating its fast convergence property.

Additional checkable conditions can be derived for Problem (ML_1) by an application of the necessary conditions given in (31). Using (31b) and (31e), it can be shown [7] that the costates satisfy the (checkable) conditions,

$$\lambda_h(t) = c_1 \quad (35a)$$

$$\lambda_v(t) = -c_1 t + c_2 \quad (35b)$$

$$\lambda_m(t_f) = 0 \quad (35c)$$

where c_1 and c_2 are some constants. A plot of the Birkhoff-generated costates is shown in Fig. 3. It apparent from this plot that the costates satisfy (35).

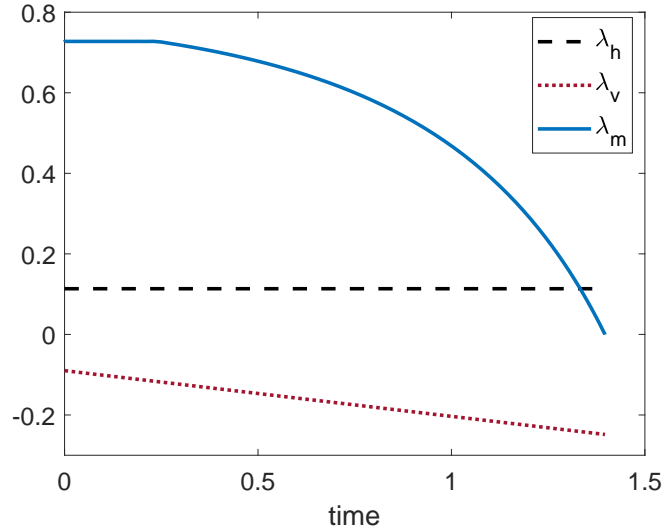


Figure 3. Birkhoff-theory-generated costates for the moon-landing problem given by (33)

B. A Problem With Discontinuous and Dirac-Delta Functions for Covector Trajectories

Consider the following deceptively simple optimal control problem [7, 53]:

$$\mathbf{x} := (x, v) \in \mathbb{R}^2 \quad \mathbf{u} := u \in \mathbb{R}$$

$$(B) \quad \left\{ \begin{array}{ll} \text{Minimize} & J[\mathbf{x}(\cdot), \mathbf{u}(\cdot)] = \frac{1}{2} \int_{t_0}^{t_f} u^2(t) dt \\ \text{Subject to} & \dot{x} = v \\ & \dot{v} = u \\ & (x_0, v_0, t_0) = (0, 1, 0) \\ & (x_f, v_f, t_f) = (0, -1, 1) \\ & x(t) \leq \ell = 0.1 \end{array} \right. \quad (36)$$

According to [53], this problem (with a generic ℓ) was originally designed by Breakwell to illustrate the various nuances of state variable inequality constraints. The solution provided in [53] is based on the original Gamkrelidze-version of Pontryagin's Principle. The solution provided in [7] is based on the Dubovitskii-Milyutin generalization [54] of Pontryagin's Principle. The basic thrust of this generalization is given by (31). Using (31) and (32), it can be shown (see Problem 4.4.3 in [7]) that the co-position trajectory, $t \mapsto \lambda_x(t)$ is given by,

$$\dot{\lambda}_x(t) = -\mu(t) = -22.22 \delta_{Dirac}(t - t_i), i = 1, 2, \quad t_1 = 0.3, t_2 = 0.7 \quad (37)$$

where, $\mu(t)$ is the path covector associated with the state constraint, $x(t) \leq 0.1$. As indicated in (37), $\mu(t)$ is given explicitly in terms of the shifted Dirac-delta functions, $\delta_{Dirac}(t - t_i)$. Furthermore, it can be shown [7] that $t \mapsto \lambda_x(t)$ is piecewise constant with downward jumps at t_1 and t_2 .

The Birkhoff-generated covector trajectories to this problem is shown in Fig. 4 for $N = 100$. It is apparent from Fig. 4 that the Birkhoff-computed solution is completely consistent with the theoretical conditions given by (37). Note,

in particular, the high-accuracy of the atomic measure captured by the Birkhoff solution, $t_k \mapsto \mu(t_k)$, $k = 0, \dots, 100$: just two points around $t_1 = 0.3$ and $t_2 = 0.7$ are off of the zero line in Fig. 4.b). These plots demonstrates that a Birkhoff-theoretic method is able to well-approximate Dirac-delta functions and produce jump discontinuities in the costates.

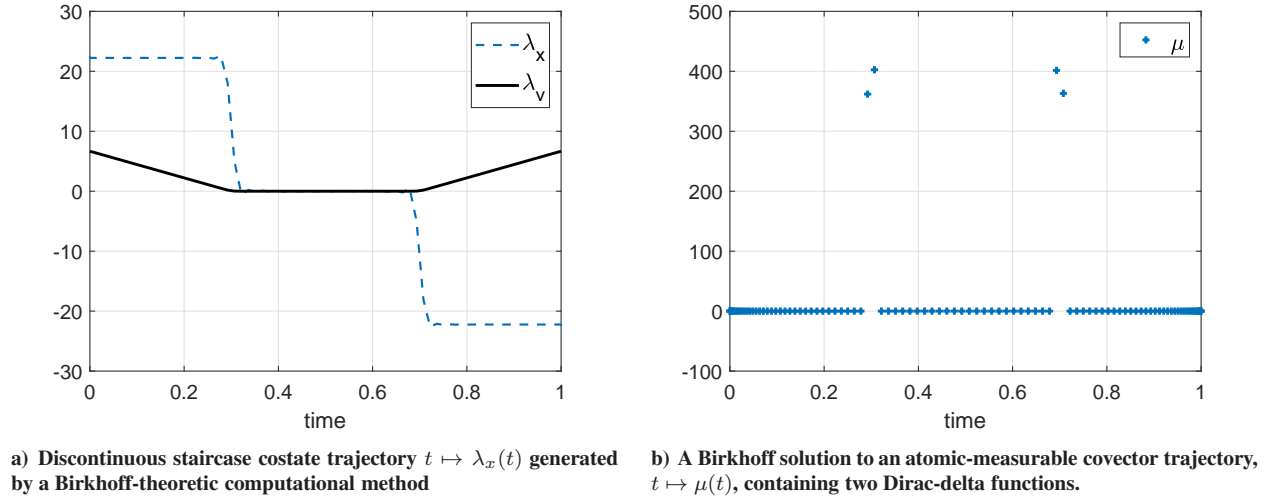


Figure 4. Birkhoff-produced discontinuous and Dirac-delta-type covector trajectories for Problem (B).

C. A Highly Oscillatory Trajectory Optimization Problem Requiring a Dense Grid

A challenge low-thrust circle-to-circle orbit transfer problem is given by [4],

$$\mathbf{x} = (r, \theta, v_r, v_t) \in \mathbb{R}^4, \quad \mathbf{u} = \alpha \in \mathbb{R}$$

$$(O_{\text{Xfer}}) \left\{ \begin{array}{ll} \text{Minimize} & J[\mathbf{x}(\cdot), \mathbf{u}(\cdot), t_f] = t_f \\ \text{Subject to} & \dot{r} = v_r \\ & \dot{\theta} = v_t/r \\ & \dot{v}_r = v_t^2/r - 1/r^2 + 5 \times 10^{-4} \sin \alpha \\ & \dot{v}_t = -v_r v_t/r + 5 \times 10^{-4} \cos \alpha \\ & t_0 = 0 \\ & (r_0, \theta_0, v_{r0}, v_{t0}) = (1, 0, 0, 1) \\ & (r_f, v_{rf}, v_{tf}) = (6, 0, \sqrt{1/6}) \end{array} \right. \quad (38)$$

where, the numerical values of the various quantities are representative of a LEO-to-GEO maneuver. What makes this particular problem challenging is that the optimal steering $t \mapsto \alpha(t)$ is highly oscillatory [4]; hence, the grid must be sufficiently dense to avoid aliasing [18, 20, 39]. If one were to use a Lagrange PS method with, say, $N \sim 500$ nodes, it is evident from Fig. 5 (see also Fig. 1 in [1]) that the “best” condition number (LGL grid) would be about 10^4 , while the worst (LGR grid) would be about 10^5 . In sharp contrast, as shown in Fig. 6, the condition number of the linear system associated with a Birkhoff PS method (i.e., $[\mathbf{A}_a(\pi^N), -\mathbf{C}_a^N]$; see (24)) is only about 22 for 500 nodes (varies almost exactly as \sqrt{N} as shown in Fig. 6.a) while that of the sub-block given by $[\mathbf{I}^N, -\mathbf{B}^a]$ flatlines to approximately 1.76. As a matter of further contrast, if one were to limit the condition number to approximately 22, then the maximum number of allowable nodes for a Lagrange PS method would be about 16 for an LGL grid and less than 10 for an LGR grid (see Fig. 5). Because the CGL/CGR grids have condition numbers that are closer to an LGL grid, the corresponding maximum number of node points for a Chebyshev grid would roughly be the same as that of an LGL grid. At such low values of N , the differences between a high-order Runge-Kutta-type collocation [55] and Lagrange PS methods become vanishingly small with the latter providing no significant advantages over the former [17, 18, 56, 57].

On the basis of the preceding analysis and the data in Fig. 6, it is apparent that producing a solution with 500 or more grid points using a Birkhoff method should not wreak havoc in the linear algebra that underpins the trajectory optimization algorithm. Indeed, a candidate primal solution to Problem (O_{Xfer}) for $N = 600$ is shown in Fig. 7. It is

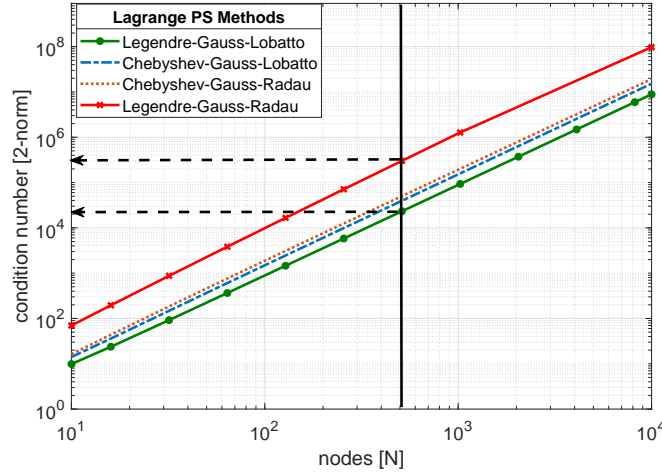
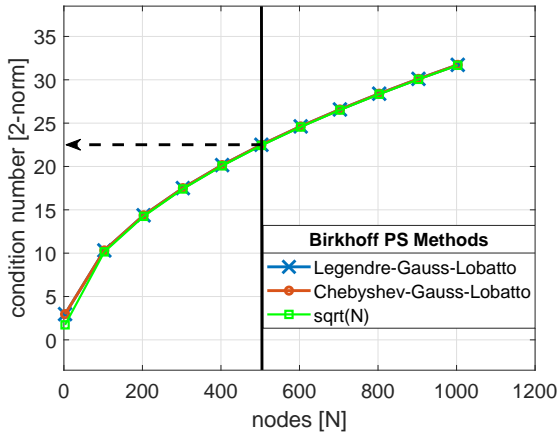
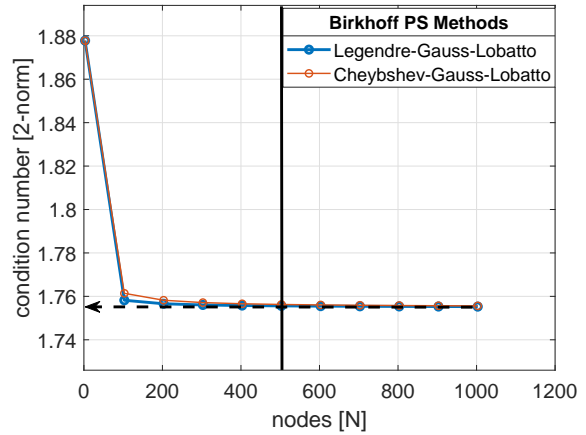


Figure 5. Condition numbers for Lagrange PS methods (cf. Fig. 1 in [1])



a) Condition numbers for the primal linear system associated with Birkhoff PS methods



b) Condition numbers for the sub-blocks given by $(I^N, -B^a)$

Figure 6. Condition numbers of Birkhoff PS methods.

apparent that the candidate optimal control is highly oscillatory which implies (by the sampling theorem [19, 20]) that a sufficiently large number of grid points are necessary to adequately represent the solution. A simple method to test the sufficiency condition is to simply solve the IVP (see (30)) generated by the candidate optimal control. A solution to this IVP is the propagated solution indicated in Fig. 7. By a cursory inspection of Fig. 7, it is clear that this solution is indeed primal feasible (see Definition 1 and Remark 4).

Beyond the issues pertaining to dense grids and condition numbers, it turns out that part of the challenges in generating an optimal low-thrust solution is that the problem is not well balanced [58]. That is, even under canonical scaling (as already performed in (38)) it turns out that the costates have very large values that range from zero to 2000. In principle, it is possible to generate a well-balanced computational problem by choosing designer units [7] as detailed in [58]; however, as shown in Fig. 8, a reasonably well-balanced Problem ($O_{X_{fer}}$) was feasible by simply scaling down the cost function by a factor of 100. Thus, for example, the values of λ_r in canonical-consistent units (see [7, 58]) has a range of about 2,000 time units per distance units. By scaling down the cost function (time units) by a factor of 100, the range of values of λ_r was brought down roughly consistent with that of r (of 6 units, per (38)). As apparent from Fig. 8, the same scale factor generated a roughly balanced problem with respect to the other primal-dual pairs, namely, (θ, λ_θ) , (v_r, λ_{v_r}) and (v_t, λ_{v_t}) . Note also that, except for λ_θ , the costates are highly oscillatory. Taken all together, i.e., grid density, oscillatory functions, condition numbers, scaling and balancing, it is clear why a low-thrust trajectory optimization problem is challenging.

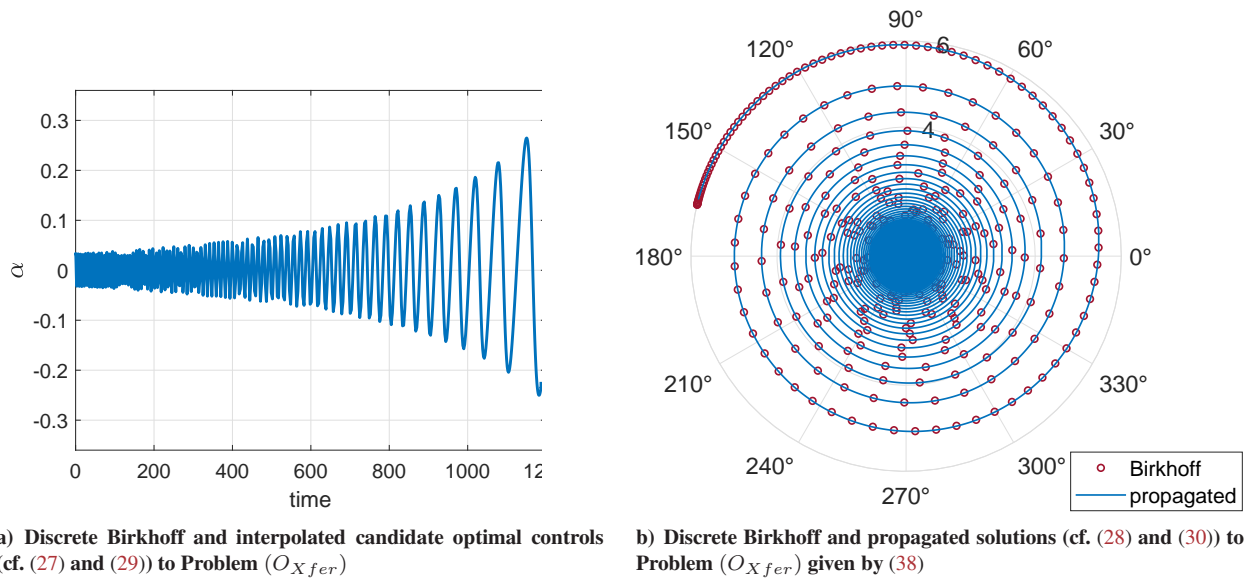


Figure 7. A Birkhoff-theoretic primal-feasible solution to Problem ($O_{X_{fer}}$)

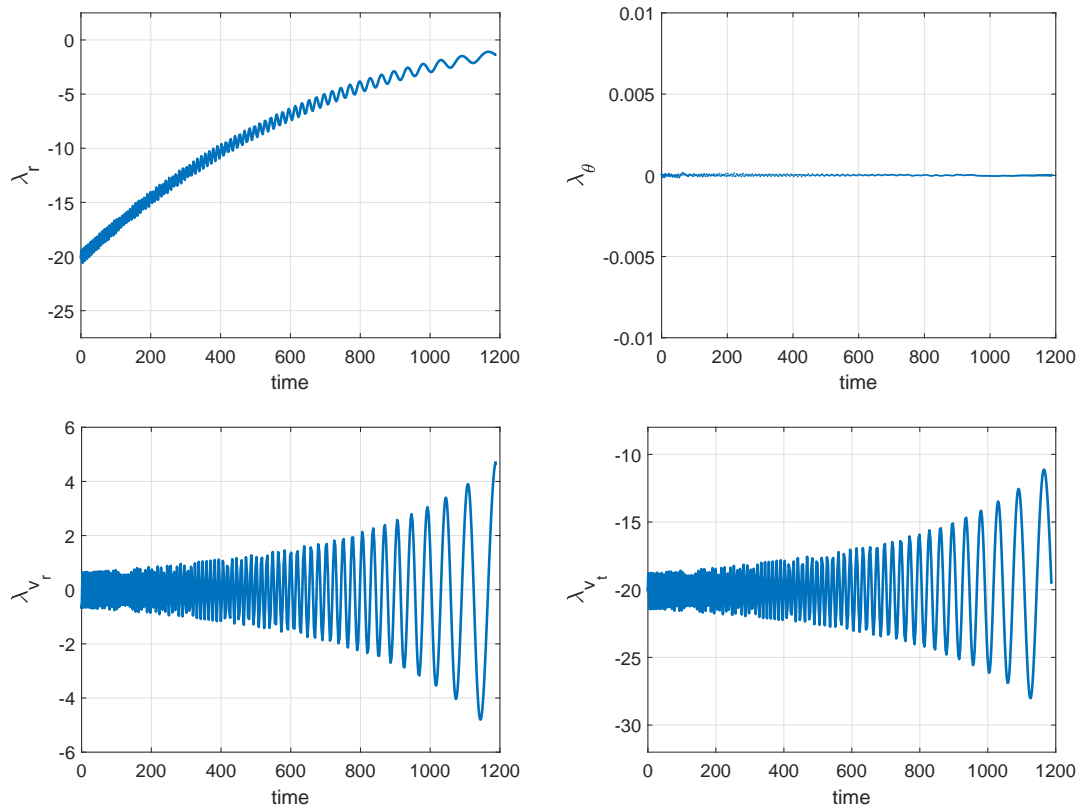


Figure 8. Highly oscillatory costate trajectories for Problem ($O_{X_{fer}}$) balanced by a scale factor of 100 in accordance with the procedure of [58].

Applying (31) to Problem ($O_{X_{fer}}$), it is straightforward to show that an optimal trajectory must satisfy the fol-

lowing necessary conditions:

$$\lambda_\theta(t) = 0 \quad (39a)$$

$$\lambda_{v_r}(t) \sin \alpha(t) + \lambda_{v_t}(t) \cos \alpha(t) \leq 0 \quad (39b)$$

$$\mathcal{H}[\alpha] = -1 \quad (39c)$$

That (39a) is satisfied is apparent from Fig. 8. The satisfaction of (39b) and (39c) over the primal-feasible solution of Fig. 7 is shown in Fig. 9. These dual optimality tests indicate that the primal feasible solution satisfies all of the

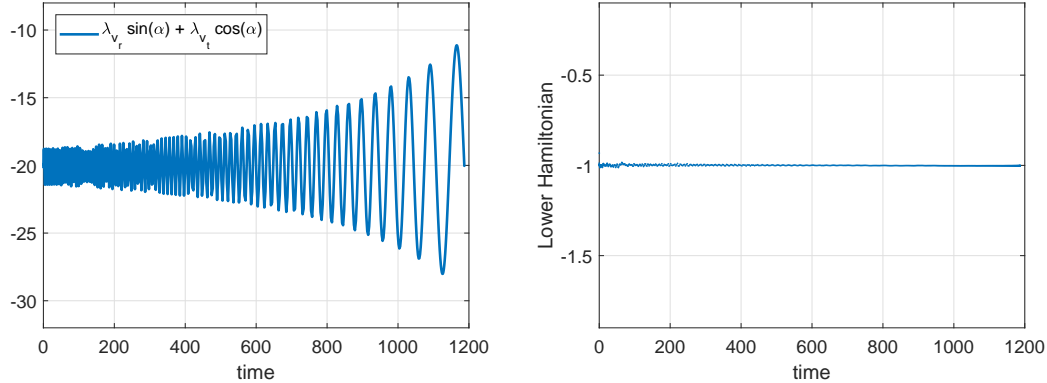


Figure 9. Plots of the left-hand-side of (39b) and (39c)

verifiable optimality conditions resulting from an application of Pontryagin’s principle. As a matter of completion, we briefly note that these verification tests were made possible by the results of Part I of this paper [1].

D. A Brief Discussion on the Totality of Results

At this juncture, it is instructive to provide a broader perspective on all of the numerical results presented. Beyond the specifics illustrated in each of the preceding example problems and solutions, the constant theme in all cases are independent demonstrations of feasibility and the satisfaction of the necessary conditions of optimality via the methods described in Section IV. It is apparent by the presentation of the results in all these cases that the CMP (derived in [1]) plays a critically important but well-hidden role. In fact, this is precisely the point of the CMP: to be not distractive in analyzing a particular problem as indicated in the left “analysis box” of Fig. 3 in [1].

Consider, for the purposes of argument, a direct method that does not satisfy the CMP. The most that can be said of a solution resulting from such a method is primal feasibility (provided it is independently validated via the methods described in Section IV). It is fairly straightforward to show, via simple examples and flight results, that the gap between feasibility and optimality can easily be 50% in propellant [59] (100% in the case of the Zero-Propellant Maneuver [60]) or 70% in maneuver time [61] (100% in the case of “FastMan,” a time-optimal maneuver [62] implemented onboard the Lunar Reconnaissance Orbiter [63]). In other words, the notion that “feasibility is sufficient for most engineering problems” is highly misguided. We also emphasize that finding optimal solutions has intrinsic value even if the optimal solution is never implemented in flight: it informs engineers and operators the price of their suboptimal/nonoptimal decisions. We finally note that a direct method (that does not satisfy the CMP) can also potentially generate false infeasibilities that might produce unsafe or dangerous human flight operations [64].

VI. Conclusions

In this part II of a two-part paper, we showed that the universal Birkhoff theory advanced in part I holds for a family of Legendre and Chebyshev grid points, be it Lobatto, Radau or Gauss. Recent advancements in spectral methods prove that all of these grid points can be generated at an $\mathcal{O}(1)$ computational speed. Nonetheless, the collection of Chebyshev grid points are the easiest to implement because it requires just about a single line of code based on the cosine function. Among the set of Birkhoff matrices generated for Lobatto, Radau and Gauss grid points, the Lobatto set has the particular property that the last row of the a -form of the Birkhoff matrix is identically equal to the Birkhoff quadrature weights. This convenience implies that the Birkhoff method over a Chebyshev-Gauss-Lobatto grid is the easiest to implement. The other five grid selections appear to be equally effective but require additional effort.

The computation of all Birkhoff matrices can be performed rapidly, efficiently and stably over thousands of grid points without suffering round-off errors that plague Lagrange pseudospectral methods; i.e., methods based on differentiation matrices. All Birkhoff matrices over the Legendre and Chebyshev grids flatten the rapid growth in the condition numbers from $\mathcal{O}(N^2)$ to $\mathcal{O}(1)$. As proved in this paper, the Birkhoff methods generated over six well-known grid points satisfy the covector mapping principle; i.e., a “direct” Birkhoff method is equivalent to an “indirect” method. This equivalence is exploited to reuse previously-developed spectral algorithms that rely on covector mapping theorems. Furthermore, as proved in part I of this paper, the Birkhoff-specific primal-dual system can be isolated to a linear system even for nonlinear problems. Because this property does not hold for Lagrange pseudospectral methods, the resulting spectral algorithm can be further customized to take advantage of this linear-nonlinear split.

It is clear from the details provided in this paper that a fast and accurate implementation of a Birkhoff method requires an integration of several disparate concepts in mathematical analysis and computational theory. This daunting task can be alleviated by selecting a Chebyshev-Gauss-Lobatto grid. This is because a Birkhoff method over this selection is the easiest to implement through the use of readily available off-the-shelf software. As illustrated in Section V of this paper, a Birkhoff method over a Chebyshev-Gauss-Lobatto grid is fully capable of solving practical problems of interest in aerospace and mechanical engineering even when the primal-dual solution involves discontinuities and Dirac-delta functions.

VII. Acknowledgment

Partial funding for this research, provided by the Defense Advanced Research Project Agency, is gratefully acknowledged.

References

- [1] I. M. Ross, “A Universal Birkhoff Theory for Fast Trajectory Optimization,” arXiv preprint *arXiv*.
- [2] I. M. Ross, R. J. Proulx, C. F. Borges, “A Universal Birkhoff Pseudospectral Method for Solving Boundary Value Problems,” *Applied Mathematics and Computation*, Vol. 454, 128101, 2023.
- [3] L.-L. Wang, M. D. Samson and X. Zhao, “A Well-Conditioned Collocation Method Using a Pseudospectral Integration Matrix,” *SIAM Journal of Scientific Computaton*, Vol. 36, No. 3, pp. A907-A929, 2014.
- [4] N. Koeppen, I. M. Ross, L. C. Wilcox and R. J. Proulx, “Fast Mesh Refinement in Pseudospectral Optimal Control,” *Journal of Guidance, Control, and Dynamics*, vol. 42 no. 4, pp. 711-722, 2018.
- [5] I. M. Ross and R. J. Proulx, “Further Results on Fast Birkhoff Pseudospectral Optimal Control Programming,” *Journal of Guidance, Control, and Dynamics*, vol. 42 no. 9, pp. 2086–2092, 2019.
- [6] I. M. Ross, “A Roadmap for Optimal Control: The Right Way to Commute,” *Annals of the New York Academy of Sciences*, 1065/1, 2005, 210–231.
- [7] I. M. Ross, *A Primer on Pontryagin’s Principle in Optimal Control*, Second Edition, Collegiate Publishers, San Francisco, CA, 2015.
- [8] Q. Gong, I. M. Ross, W. Kang and F. Fahroo, “On the Pseudospectral Covector Mapping Theorem for Nonlinear Optimal Control,” *Proceedings of the 45th IEEE Conference on Decision and Control*, 2006, pp. 2679-2686, doi: 10.1109/CDC.2006.377729.
- [9] I. M. Ross, “A Historical Introduction to the Covector Mapping Principle,” *Advances in the Astronautical Sciences*, Vol. 123, Univelt, San Diego, CA, 2006, pp. 1257–1278.
- [10] I. M. Ross and F. Fahroo, “A Perspective on Methods for Trajectory Optimization,” *AIAA/AAS Astrodynamics Specialist Conference and Exhibit*, 5-8 August, 2002, Monterey, CA. AIAA 2002-4727. <https://doi.org/10.2514/6.2002-4727>.
- [11] Fahroo, F., and Ross, I. M., “Costate estimation by a Legendre pseudospectral method,” *AIAA Journal of Guidance, Control and Dynamics*, Vol. 24, No. 2, pp. 270-277, 2001.
- [12] I. M. Ross and F. Fahroo, “Discrete Verification of Necessary Conditions for Switched Nonlinear Optimal Control Systems,” *Proceedings of the American Control Conference*, June 2004, Boston, MA.

- [13] F. Fahroo and I. M. Ross, "Advances in Pseudospectral Methods for Optimal Control," *AIAA Guidance, Navigation, and Control Conference*, AIAA Paper 2008-7309, Honolulu, Hawaii, August 2008.
- [14] Q. Gong, I. M. Ross and F. Fahroo, "Costate Computation by a Chebyshev Pseudospectral Method," *Journal of Guidance, Control and Dynamics*, Vol. 33, No. 2, pp. 623-628, 2010.
- [15] Q. Gong, I. M. Ross and F. Fahroo, "Pseudospectral Optimal Control On Arbitrary Grids," *AAS Astrodynamics Specialist Conference*, AAS-09-405, 2009.
- [16] Q. Gong, I. M. Ross and F. Fahroo, "Spectral and Pseudospectral Optimal Control Over Arbitrary Grids," *Journal of Optimization Theory and Applications*, vol. 169, no. 3, pp. 759-783, 2016.
- [17] I. M. Ross and M. Karpenko, "A Review of Pseudospectral Optimal Control: From Theory to Flight," *Annual Reviews in Control*, Vol.36, No.2, pp.182-197, 2012.
- [18] B. Fornberg, *A Practical Guide to Pseudospectral Methods*. Cambridge University Press Cambridge, 1996.
- [19] J. Boyd, *Chebyshev and Fourier Spectral Methods*, Dover Publications, Inc., Minola, New York, 2001.
- [20] L. N. Trefethen, *Spectral Methods in MATLAB*. SIAM, Philadelphia, PA, 2000.
- [21] Hesthaven, J., Gottlieb, S., Gottlieb, D., *Spectral Methods for Time-Dependent Problems* Cambridge Monographs on Applied and Computational Mathematics, Cambridge University Press, Cambridge, UK, 2007.
- [22] J. S. Hesthaven, "Integration Preconditioning Of Pseudospectral Operators. I. Basic Linear Operators," *SIAM Journal of Numerical Analysis*, Vol. 35, No. 4, pp. 1571-1593, 1998.
- [23] E. M. E. Elbarbary, "Integration Preconditioning Matrix for Ultraspherical Pseudospectral Operators," *SIAM Journal of Scientific Computaton*, Vol. 28, No. 3, pp. 1186-1201, 2006.
- [24] L. N. Trefethen, *Approximation Theory and Approximation Practice*, SIAM, Philadelphia, PA, 2013.
- [25] I. Bogaert, Iteration-Free Computation of Gauss-Legendre Quadrature Nodes and Weights, *SIAM J. Sci. Comput.*, 36/3 (2014), A1008-A1026.
- [26] L.-L. Wang, B.-Y. Guo, "Interpolation approximations based on Gauss-Lobatto-Legendre-Birkhoff quadrature," *Journal of Approximation Theory*, Volume 161, Issue 1, 2009, Pages 142-173.
- [27] L. N. Trefethen, "Is Gauss Quadrature Better than Clenshaw-Curtis?" *SIAM Review*, Vol. 50, No. 1, pp. 67-87, 2008.
- [28] J. Waldvogel, "Fast Construction of the Fejér and Clenshaw-Curtis Quadrature Rules," *BIT Numerical Mathematics*, 46, 2006, pp. 195-202.
- [29] F. Fahroo and I. M. Ross, "Convergence of the Costates Does Not Imply Convergence of the Control," *Journal of Guidance, Control and Dynamics*, Vol. 31, No. 5, pp. 1492-1497, 2008.
- [30] Karpenko, M., Bhatt, S., Bedrossian, N., Ross, I. M., "Flight Implementation of Shortest-Time Maneuvers for Imaging Satellites," *Journal of Guidance, Control and Dynamics*, Vol. 37, No. 4, pp. 1069-1079, 2014.
- [31] N. Bedrossian, S. Bhatt, W. Kang, I. M. Ross, "Zero Propellant Maneuver Guidance," *IEEE Control Systems Magazine*, Vol. 29, Issue 5, October 2009, pp. 53-73.
- [32] N. Bedrossian, M. Karpenko, and S. Bhatt, "Overclock My Satellite: Sophisticated Algorithms Boost Satellite Performance on the Cheap," *IEEE Spectrum Magazine*, Vol. 49, No. 11, 2012, pp. 54-62.
- [33] Q. Gong, F. Fahroo and I. M. Ross, "Spectral Algorithm for Pseudospectral Methods in Optimal Control," *Journal of Guidance, Control, and Dynamics*, vol. 31 no. 3, pp. 460-471, 2008.
- [34] Q. Gong and I. M. Ross, "Autonomous Pseudospectral Knotting Methods for Space Mission Optimization," *Advances in the Astronautical Sciences*, Vol. 124, 2006, AAS 06-151, pp. 779-794.
- [35] I. M. Ross, "Enhancements to the DIDO Optimal Control Toolbox," arXiv preprint, arXiv:2004.13112, 2020, <https://arxiv.org/abs/2004.13112>

- [36] I. M. Ross and F. Fahroo, "Pseudospectral Knotting Methods for Solving Optimal Control Problems," *Journal of Guidance, Control and Dynamics*, Vol. 27, No. 3, pp. 397-405, 2004.
- [37] Ross, I. M., D'Souza, C. N., "Hybrid Optimal Control Framework for Mission Planning," *Journal of Guidance, Control and Dynamics*, Vol. 28, No. 4, pp. 686-697, 2005.
- [38] I. M. Ross, F. Fahroo and J. Strizzi, "Adaptive Grids for Trajectory Optimization by Pseudospectral Methods," *AAS/AIAA Spaceflight Mechanics Conference*, Paper No. AAS 03-142, Ponce, Puerto Rico, 9-13 February 2003.
- [39] I. M. Ross, Q. Gong and P. Sekhavat, "Low-Thrust, High-Accuracy Trajectory Optimization," *Journal of Guidance, Control and Dynamics*, Vol. 30, No. 4, pp. 921-933, 2007.
- [40] I. M. Ross, Q. Gong and P. Sekhavat, "The Bellman Pseudospectral Method," *AIAA/AAS Astrodynamics Specialist Conference and Exhibit*, Honolulu, Hawaii, AIAA-2008-6448, August 18-21, 2008.
- [41] F. Fahroo and I. M. Ross, "Pseudospectral Methods for Infinite-Horizon Nonlinear Optimal Control Problems," *Proceedings of the AIAA Guidance, Navigation and Control Conference*, San Francisco, CA, August 15-18, 2005.
- [42] I. M. Ross, Q. Gong, F. Fahroo and W. Kang, "Practical stabilization through real-time optimal control," *Proceedings of the 2006 American Control Conference*, Inst. of Electrical and Electronics Engineers, Piscataway, NJ, June 2006, pp. 14-16.
- [43] F. Fahroo and I. M. Ross, "Pseudospectral Methods for Infinite-Horizon Optimal Control Problems," *Journal of Guidance, Control and Dynamics*, Vol. 31, No. 4, pp. 927-936, 2008.
- [44] T. A. Driscoll, N. Hale, and L. N. Trefethen, editors, *Chebfun Guide*, Pafnuty Publications, Oxford, 2014.
- [45] W. Chen, Z. Shao and L. T. Biegler, "A Bilevel NLP Sensitivitybased Decomposition for Dynamic Optimization with Moving Finite Elements," *AIChE J.*, 2014, 60, 966-979.
- [46] W. Chen and L. T. Biegler, "Nested Direct Transcription Optimization for Singular Optimal Control Problems," *AIChE J.*, 2016, 62, 3611-3627.
- [47] L. Ma, Z. Shao, W. Chen and Z. Song, "Trajectory optimization for lunar soft landing with a Hamiltonian-based adaptive mesh refinement strategy," *Advances in Engineering Software* Volume 100, October 2016, pp. 266-276.
- [48] I. M. Ross, "A Direct Shooting Method is Equivalent to An Indirect Method," arXiv preprint (2020) arXiv:2003.02418.
- [49] H. Yan, Q. Gong, C. Park, I. M. Ross, and C. N. D'Souza, "High Accuracy Trajectory Optimization for a Trans-Earth Lunar Mission," *Journal of Guidance, Control and Dynamics*, Vol. 34, No. 4, 2011, pp. 1219-1227.
- [50] S. Bhatt, N. Bedrossian, K. Longacre and L. Nguyen, "Optimal Propellant Maneuver Flight Demonstrations on ISS," *AIAA Guidance, Navigation, and Control Conference*, August 19-22, 2013, Boston, MA. AIAA 2013-5027.
- [51] G. Minelli, M. Karpenko, I. M. Ross and J. Newman, "Autonomous Operations of Large-Scale Satellite Constellations and Ground Station Networks," *AAS/AIAA Astrodynamics Specialist Conference*, August 20 - 24, 2017 Stevenson, WA. AAS-17-761
- [52] J. S. Meditch, "On the Problem of Optimal Thrust Programming for a Lunar Soft Landing," *IEEE Transactions on Automatic Control*, AC-9, No. 4, pp. 477-484, 1964
- [53] Bryson, A. E., and Ho, Y.-C., *Applied Optimal Control*, Hemisphere, New York, 1975 (Revised Printing; original publication, 1969).
- [54] Dmitruk, A., Samylovskiy, I., "On the relation between two approaches to necessary optimality conditions in Problems with State Constraints," *J. Optim. Theory Appl.*, 173(2), 391-420 (2017)
- [55] A. Herman and B. A. Conway, "Direct Optimization Using Collocation Based on High-Order Gauss-Lobatto Quadrature Rules," *Journal of Guidance Control and Dynamics*, Vol.39, No.3, 1996, pp.592-599.
- [56] B. A. Conway, "A Survey of Methods Available for the Numerical Optimization of Continuous Dynamic Systems," *Journal of Optimization Theory and Applications*, Vol. 152, 2012, pp. 271-306.

- [57] E. Hairer, S. P. Nørsett, G. Wanner, *Solving Ordinary Differential Equations I: Nonstiff Problems*, Springer-Verlag Berlin Heidelberg, 1993.
- [58] I. M. Ross, Q. Gong, M. Karpenko and R. J. Proulx, “Scaling and Balancing for High-Performance Computation of Optimal Controls,” *Journal of Guidance, Control and Dynamics*, Vol. 41, No. 10, 2018, pp. 2086–2097.
- [59] Ross, I. M., “How to Find Minimum-Fuel Controllers,” *AIAA Guidance, Navigation, and Control Conference and Exhibit*, AIAA Paper 2004-5346, 2004.
- [60] N. Bedrossian, S. Bhatt, M. Lammers and L. Nguyen, “Zero Propellant Maneuver: Flight Results for 180° ISS Rotation,” *20th International Symposium on Space Flight Dynamics*, September 24-28, 2007, Annapolis, MD, NASA/CP-2007-214158.
- [61] A. Fleming, P. Sekhavat, and I. M. Ross, “Minimum-Time Reorientation of a Rigid Body,” *Journal of Guidance, Control, and Dynamics*, Vol. 33, No.1, Jan-Feb 2010, pp. 160–170.
- [62] Karpenko, M., Lippman, T., Ross, I.M., Halverson, J.K., McClanahan, T., Barker, M., Mazarico, E., Besser, R., Dennehy, C.J., VanZwieten, T., and Wolf, A., “Fast Attitude Maneuvers for the Lunar Reconnaissance Orbiter,” *42nd Annual AAS Guidance & Control Conference*, Jan. 31 to Feb. 6, 2019, Breckenridge, CO. Paper number: AAS 19-053.
- [63] Johnston, S. A., “Lunar Reconnaissance Orbiter gets an upgrade to capture new perspectives of the moon,” *Universe Today*, February 15, 2021, <https://phys.org/news/2021-02-lunar-reconnaissance-orbiter-capture-perspectives.html>
- [64] K. P. Bollino, *High-Fidelity Real-Time Trajectory Optimization for Reusable Launch Vehicles*, Ph.D. Dissertation, Naval Postgraduate School, Monterey, CA, Dec 2006.